https://doi.org/10.22226/2410-3535-2022-2-137-141

Formation of a pore as stress relaxation mechanism in decahedral small particles

S. A. Krasnitckii[1], M. Yu. Gutkin[†,1], A. L. Kolesnikova[1,2], A. E. Romanov[1]

[†]m.y.gutkin@gmail.com

[1]National Research University of Information Technologies, Mechanics, and Optics (ITMO University), St. Petersburg, 197101, Russia
[2]Institute for Problems in Mechanical Engineering, RAS, St. Petersburg, 199178, Russia

A theoretical model of mechanical stress relaxation in decahedral particles by the formation of a central spherical pore is suggested and analyzed within an energy approach. The strain energy of a hollow decahedral particle is found in a closed analytical form. It is shown that there is a critical radius of a decahedral particle below which the formation of a central pore is not energetically favorable, while above which it is. The optimal radius of the pore increases with growth of the particle. Theoretical results are verified with available experimental data on observation of hollow decahedral particles.

Keywords: nanostructure, residual stresses, stress relaxation, disclinations, hollow decahedral nanoparticles.

1. Introduction

In the last two decades, hollow and porous nano- and microstructures attracted a keen interest in various research fields and practical applications, e. g. see reviews [1–4]. However, few attempts were focused on the theoretical aspects of pore/void formation in nano- and microparticles [5]. The processes of pore nucleation and evolution in such objects can be driven by different factors including structural crystallinity [5], diffusivity of components [6], presence of vacancy sinks/sources [7], surface and volume stress states [8], etc.

A great amount of available experimental data on pore formation in nano- and microobjects get focused on the phenomenon observed in pentagonal crystals (PCs) [9–14]. The building of PCs, also known as multiply twinned particles (MTPs), is controlled by five-fold cycling twinning in materials with FCC crystal structure [15,16]. Pentagonal crystals exist in the form of pentagonal wires (PWs), decahedral small particles (DSPs) and icosahedral small particles (ISPs). It is worth mentioning that hollows in MTPs are produced by different strategies using electrodeposition [10–12], chemical etching [17] and surfactants [18], galvanic [19] and Kirkendall [20] replacement of components, and electron beam irradiation [21,22]. The pore formation in MTPs was first theoretically described for PWs and ISPs (but not for DSPs) in Ref. [9] as an efficient channel of residual mechanical stress relaxation.

Nowadays the residual stresses being inherent to MTPs are well understood in the framework of disclination approach [23,24] originating from pioneering works by De Wit [25] and Galligan [26]. In the disclination approach, the inhomogeneous stress/strain state in MTPs is caused by wedge disclinations (WDs) [15,23]. In accordance with this approach, five tetrahedral material domains with FCC crystalline structure and with {111}-type crystallographic planes surface facets are glued together around an edge, which coincides with <011>-type crystallographic direction, to form a DSP in the form of a polyhedron with ten triangular facets, i. e. decahedron. Domains inside the DSP are separated by five coherent twin boundaries. Their common five-fold junction contains a partial positive WD of strength $\omega \approx 0.128$ rad. Similar model treats PWs as pentagonal prisms elongated in <011>-type crystallographic direction and having {100}-type crystallographic planes on lateral prism facets and WDs of strength ω along the prism axes. In a similar way, ISPs are treated as icosahedra with six WDs of strength ω connecting opposite vertices of the icosahedra [15,23].

The continuum models suitable for the analysis of stresses and stored strain energy in MTPs, consider a DSP and an ISP as an elastic sphere containing either a single positive WD or six such WDs, correspondingly, and a PW as an elastic cylinder with a single WD. Whereas elastic properties of WDs in a cylinder were studied in numerous textbooks on Mechanics of Solids [27,28], there exist only few solutions for WDs in the bodies with spherical symmetry. Polonsky et al. [29] were the first who found elastic fields and energy of such a WD in an elastic sphere. Recently, Kolesnikova et al. [30] extended this solution to the case of a WD in a hollow sphere.

In the present paper, we employ the solution [30] to find analytical expressions for strain energies stored in both solid and hollow DSPs. Based on these results, we suggest a theoretical model of residual stress relaxation due to the pore formation in disclinated DSPs. (The idea about the diminishing of the WD energy via the formation the void in its core was advanced in Ref. [31] with no relation to MTPs.)

2. Model

To model strain-stress state in an initially solid DSP (Fig. 1a) we use an elastic sphere of radius a_0, with shear modulus G and Poisson ratio ν, containing an axial positive partial WD with strength $\omega = 0.128$ rad (Fig. 1b). Within such a model, the interior region of DSP is compressed while the periphery region is stretched with the exception of small compressed regions around the poles crossed by the disclination line (see Fig. 8 in Ref. [30] for details). We expect that such residual stress state causes the generation of vacancies on the DSP stretched surface and their migration to the DSP compressed interior region with subsequent coagulation to form a central spherical pore of radius a_p (see Fig. 1c). Besides, we assume that the inverse migration flow of atoms from the compressed interior region of the DSP to its outer surface leads to an increase in the DSP visible volume. This volume increase can be described in terms of radii $a^3 = a_0^3 + a_p^3$, where a is the radius of the DSP in its final relaxed state.

The pore formation in the interior region of a DSP leads to the following factors of its energy change: (i) an increase in its free surface area, (ii) a decrease in its twin boundaries area, (iii) strain relaxation, and (iv) radial displacement of surface atoms due to the surface tension. As it was shown earlier [9], the contribution of twin boundaries and surface tension in the total energy of both solid and hollow DSPs can be neglected.

3. Results and Discussion

The energy change of DSP due to the pore formation can be written as $\Delta E = \Delta E_{surf} + \Delta E_{strain}$, where ΔE_{surf} and ΔE_{strain} are the surface and strain energy changes, respectively. The surface term is given by $\Delta E_{surf} = \gamma(S_h - S_s)$, where γ is the free-surface specific energy, S_h and S_s are the surface areas for hollow and solid DSPs. In most practical cases, the real shape of DSPs is different from the spherical one. One can derive the surface area of a solid DSP in terms of the radius a_0 as area of ten {111}-type facets (see Fig. 1a): $S_s = 10\sqrt{3}\,a_0^2/3$. If both the pore and DSP have a faceting decahedral shape, the approximations $S_h \approx 6(a_p^2 + a^2)$ and $S_s \approx 6a_0^2$ seem reliable for theoretical estimation. Within the work, the facet representation is employed to calculate the surface energy of DSPs while the continuum model of an elastic sphere containing a WD is used to calculate the strain energy of DSPs.

To find ΔE_{strain}, let us first determine the strain energy of a WD, symmetrically piercing an elastic spherical shell, as a work spent to the creation of the WD in its own stress field:

$$ {}^{sh}E_{el}^{\omega} = \frac{\omega}{2}\int_{a_p}^{a}\int_{0}^{\pi} R^2\, {}^{sh}\sigma_{\varphi\varphi}^{\omega}\, \sin\theta\, dR d\theta, \qquad (1)$$

where the hoop stress ${}^{sh}\sigma_{\varphi\varphi}^{\omega}$ was calculated in [30]. In the present work, we reconsider the solution [30] to rewrite ${}^{sh}\sigma_{\varphi\varphi}^{\omega}$ in the following form:

$$\begin{aligned} {}^{sh}\sigma_{\varphi\varphi}^{\omega} &= \frac{G\omega}{2\pi(1-\nu)}\left(1+\ln\frac{R}{a\sin\theta}\right)+ \\ &+2G\sum_{m=0}^{+\infty}(\alpha_{1m}A_mR^{2m}+\beta_{1m}B_mR^{2m-2}+\gamma_{1m}C_mR^{-2m-1}+ \\ &\quad +\delta_{1m}D_mR^{-2m-3})P_{2m}(\cos\theta)+ \\ &+2G\sum_{m=0}^{+\infty}(\alpha_{2m}A_mR^{2m}+\beta_{2m}B_mR^{2m-2}+\gamma_{2m}C_mR^{-2m-1}+ \\ &\quad +\delta_{2m}D_mR^{-2m-3})\cot\theta P_{2m}^{1}(\cos\theta), \end{aligned} \qquad (2)$$

where $\alpha_{1m} = 2(2m+1)(m-1-\nu-4m\nu)$, $\beta_{1m} = 2m$, $\gamma_{1m} = 2m\times$ $\times(2m+3-2\nu-8m\nu)$, $\delta_{1m} = -2m-1$, $\alpha_{2m} = 2m+5-4\nu$, $\beta_{2m} = 1$, $\gamma_{2m} = -2m+4-4\nu$, $\delta_{2m} = 1$, $P_n(x)$ is the Legendre polynomial, $P_n^1(x) = -(1-x^2)^{1/2}dP_n(x)/dx$ is the associated Legendre polynomials, and $x = \cos\theta$. The expansion coefficients A_m, B_m, C_m, and D_m can be found from the following set of algebraic equations issued from the boundary conditions at $R = a_p$ and $R = a$ [30]:

$$\frac{\omega(1+\nu)}{36\pi(1-\nu)G}\left(5-6\ln\frac{2R}{a}\right)\Big|_{R=a_p,a}+2A_0(1+\nu)-2\frac{D_0}{R^3}\Big|_{R=a_p,a}=0 \qquad (3)$$

for $m = 0$, and

$$\begin{aligned} &\sigma_m\big|_{R=a_p,a}+\alpha_{3m}A_mR^{2m}\big|_{R=a_p,a}+\beta_{3m}B_mR^{2m-2}\big|_{R=a_p,a}+ \\ &\quad +\gamma_{3m}C_mR^{-2m-1}\big|_{R=a_p,a}+\delta_{3m}D_mR^{-2m-3}\big|_{R=a_p,a}=0, \end{aligned} \qquad (4a)$$

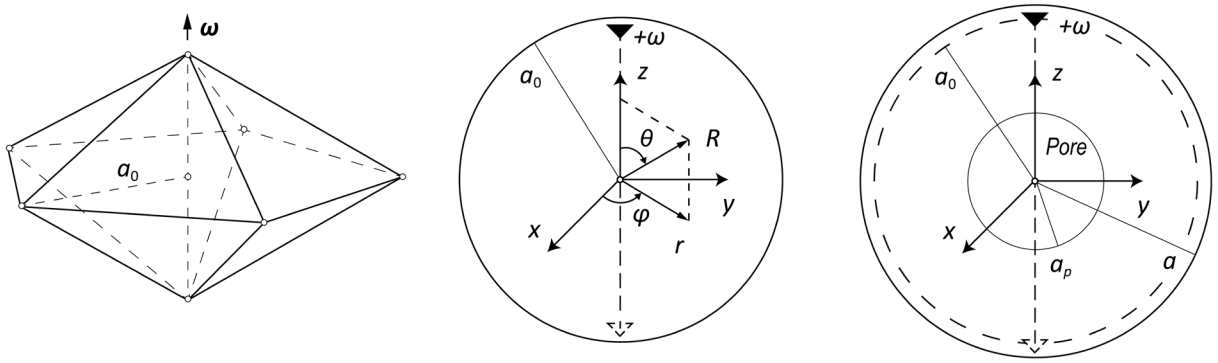

a b c

Fig. 1. Schematics of a decahedral small particle (DSP) and its elastic model: geometry of a DSP with crystallographic facets (a), solid sphere with a wedge disclination as DSP model (b), partially relaxed state with a central spherical pore (c). The Cartesian (x, y, z), cylindrical (r, φ, z) and spherical (R, θ, φ) coordinate systems are shown.

$$\tau_m\Big|_{R=a_p,a}+\alpha_{4m}A_mR^{2m}\Big|_{R=a_p,a}+\beta_{4m}B_mR^{2m-2}\Big|_{R=a_p,a}+$$
$$+\gamma_{4m}C_mR^{-2m-1}\Big|_{R=a_p,a}+\delta_{4m}D_mR^{-2m-3}\Big|_{R=a_p,a}=0, \quad (4b)$$

for $m\geq 1$, where $\alpha_{3m}=2(2m+1)(2m^2-m-1-\nu)$, $\beta_{3m}=2m(2m-1)$, $\gamma_{3m}=-4m(2m^2+3m-\nu)$, $\delta_{3m}=2(2m+1)(m+1)$, $\alpha_{4m}=4m^2+4m-1+2\nu$, $\beta_{4m}=2m-1$, $\gamma_{4m}=4m^2-2+2\nu$, $\delta_{4m}=-2(m+1)$, and (in units of $\omega/[4\pi(1-\nu)G]$):

$$\sigma_{m=1}=\frac{1}{3}\left\{1-5\nu+(1-2\nu)\left(\frac{1}{15}-2\ln\frac{2R}{a}\right)\right\},$$

$$\tau_{m=1}=\frac{1}{3}\left\{1-\nu+(1-2\nu)\left(\frac{1}{30}-\ln\frac{2R}{a}\right)\right\},$$

$$\sigma_{m=2,3,\ldots}=\frac{4m+1}{2m(2m+1)}\left\{\frac{(1-2\nu)(2m-1)(m+1)}{(2m+3)(m-1)}-1\right\},$$

$$\tau_{m=2,3,\ldots}=\frac{(1-2\nu)(4m+1)}{2m(m-1)(2m+1)(2m+3)}.$$

Eqs. (2) – (4) were obtained by using the same procedure as in [30], with the only difference that the stress field of a WD in an elastic cylinder (instead of that in an infinite elastic medium) was employed to construct the solution of the problem.

Substitution of Eq. (2) in (1) gives:

$${}^{sh}E_{el}^{\omega}=\frac{G\omega^2a^3}{18\pi(1-\nu)}\left\{\frac{2+5\nu}{3}+(1-2\nu)\ln 2-\left(\frac{2+5\nu}{3}+(5+2\nu)\ln 2\right)t^3-\right.$$
$$\left.-(1-2\nu)t^3\ln t-3(1+\nu)\frac{t^3}{1-t^3}\ln^2 t\right\}-$$
$$-2G\omega\left\{A_1\frac{7-4\nu}{5}R^5+B_1\frac{R^3}{3}+2C_1(1-2\nu)\ln R-D_1\frac{R^{-2}}{2}+\right.$$
$$\left.+\sum_{m=2}^{+\infty}(\alpha_{5m}A_mR^{2m+3}+\beta_{5m}B_mR^{2m+1}+\gamma_{5m}C_mR^{-2m+2}+\right.$$
$$\left.\left.+\delta_{5m}D_mR^{-2m})\right\}\right|_{R=a_p}^{R=a}, \quad (5)$$

where $t=a_p/a$, $\alpha_{5m}=(2m+5-4\nu)/(2m+3)$, $\beta_{5m}=1/(2m+1)$, $\gamma_{5m}=(m-2+2\nu)/(m-1)$, and $\delta_{5m}=-1/(2m)$.

In the limiting case of a solid elastic sphere ($a_p\to 0$), the corresponding strain energy of the WD acquires the following concise form:

$${}^{sp}E_{el}^{\omega}=\frac{G\omega^2a^3}{2\pi(1-\nu)}\left[\frac{1}{6}-\frac{2\nu(1+3\nu)}{15(7+5\nu)}-\right. \quad (6)$$
$$\left.-\sum_{m=2}^{\infty}\frac{(1+4m)(32m^4\nu^2-8m^3(\nu^2-7\nu+1)-4m^2(1-\nu)+2m(11\nu^2-7\nu-9)-(1+\nu)(5-4\nu))}{(m-1)2m(2m-1)(3+8m+4m^2)^2(1+\nu+2(1+\nu)m+4m^2)}\right]$$

which coincides with the result by Polonsky et al. [29].

In Fig. 2, we show the dependence of the ratio of the energy terms ${}^{sh}E_{el}^{\omega}$ and ${}^{sp}E_{el}^{\omega}$ given by Eqs. (5) and (6), respectively, on the radii ratio a_p/a for $\nu=0.35$. These dependences coincide with the results obtained by Kolesnikova in 2016 (unpublished). Similar curves obtained earlier for a hollow PW, modeled as an elastic cylindrical shell containing an axial straight WD, and for a hollow ISP, modeled as an elastic spherical shell containing a Marks-Ioffe stereo disclination [9], are shown in Fig. 2 as well. As is seen, for all the cases under consideration (for DSP, PW, and ISP), the strain energy decreases with an increase in the pore radius. Moreover, at the same value of the inner to outer radii ratio, the strain energy ratio ${}^{sh}E_{el}^{\omega}/{}^{sp}E_{el}^{\omega}$ takes the lowest value for PWs, a medium value for ISPs, and the highest value for DSPs. For example, at $a_p/a=0.5$, these values are as follows: ≈0.1 for PWs, ≈0.25 for ISPs, and ≈0.55 for DSPs. Thus, hollow DSPs store significantly higher strain energy with respect to solid DSPs, than hollow PWs and ISPs of the same inner and outer radii with respect to their solid counterparts. It is worth noting, however, that the strain energy values for a ISP treated as an elastic sphere containing six positive WDs [23] will differ from those obtained within the Marks-Ioffe model for the ISP.

Coming back to the surface and strain energy contributions in the relaxation process due to the pore formation in a DSP, we have the corresponding energy change as a function of the initial DSP radius a_0 and the pore radius a_p: $\Delta E\approx 6\gamma(a_p^2+a^2-a_0^2)+$ $+{}^{sh}E_{el}^{\omega}-{}^{sp}E_{el}^{\omega}$, where the two last terms are given by Eqs. (5) and (6), respectively. The dependence $\Delta E(a_p/a)$ is shown in Fig. 3 for different values of a_0. On the plot, the left scale shows the ΔE values in units of Gb^2a, while the right scale shows

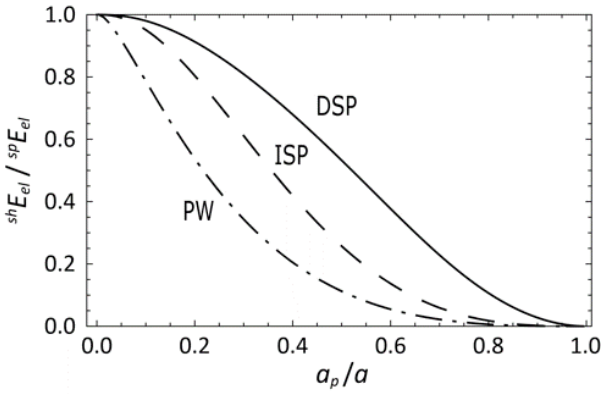

Fig. 2. The dependence of the ratio of strain energies of hollow structures to solid ones on the inner to outer radii ratio a_p/a for DSP (solid curve), ISP (dashed curve) and PW (dash-dotted curve).

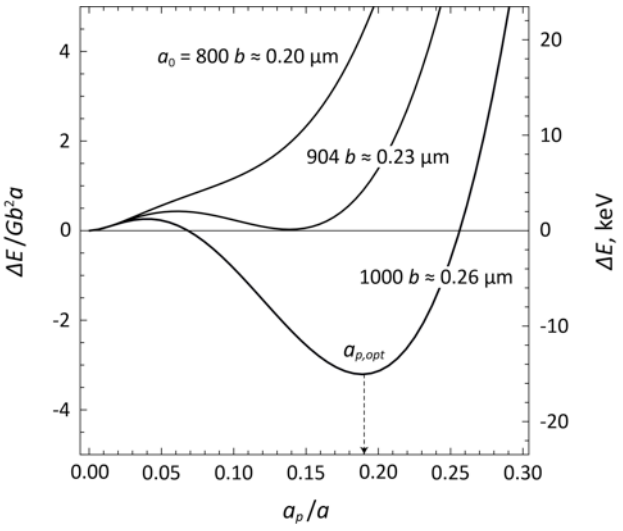

Fig. 3. The dependence of the energy change of a DSP due to pore formation on the inner to outer radii ratio for three different values of the initial radius a_0. The energy change is given for pure Cu in units of Gb^2a (the left scale) and keV (the right scale).

them in keV for the practical case of pure Cu with $\nu = 0.38$, $b = 0.256$ nm, $G = 42.8$ GPa [32] and $\gamma_{111} = 1.952$ J/m^2 [33]. The pore formation is energetically favorable if $\Delta E < 0$. As is seen from Fig. 3, there is a critical radius $a_{0,cr}$ of the initially solid DSP, such as, in DSPs with relatively small radius $a_0 < a_{0,cr}$, the pore formation is energetically unfavorable ($\Delta E > 0$ for any value of a_p), while in DSPs with relatively large radius $a_0 > a_{0,cr}$, it is energetically favorable ($\Delta E < 0$ in a range of variable a_p). It means that, in relatively small DSPs, the pore is unstable and tends to shrinkage as was observed in Au and Ag DSPs of 30 – 40 nm in diameter with pores of 3 – 8 nm in diameter [21, 22]. The critical value of the DSP radius $a_{0,cr}$ can be determined numerically from the system of equations $\Delta E = 0$, $\partial \Delta E / \partial a_0$, and $\partial^2 \Delta E / \partial a_0^2 > 0$. In our example, $a_{0,cr} \approx 904b$ in the normalized case and ≈0.23 μm for Cu (see Fig. 3).

It is worth noting that the critical radius of DSPs for generation of circular prismatic dislocation loops was earlier calculated as $\approx 258b$ [34] that is smaller than our current result for pore formation. One can conclude from this comparison that supersaturation of vacancies in center regions of growing DSPs should first lead to generation of vacancy-type prismatic dislocation loop(s) and only then to subsequent formation of a pore, probably from the loop(s). The latter process needs a special consideration that is out of scope of the present paper.

In DSPs of radius $a_0 > a_{0,cr}$, the pore tends to grow up to an optimal radius $a_p = a_{p,opt}$ corresponding to the minimum of $\Delta E < 0$ (see Fig. 3). As is seen from Fig. 3, the more the initial radius a_0 of the DSP rises, the more the optimal normalized radius $a_{p,opt}/a$ of the pore is. Besides, Fig. 4 demonstrates how the latter varies with the final radius a of DSPs, ISPs and PWs in the case of pure Cu. It is seen that, for all MTPs under consideration, the curves first sharply increase (for DSPs, at a in the range from ≈0.5 to ≈2 μm) and then smoothly grow with a. This result agrees well with experimental observation of large hollow DSPs and ISPs of radius $a > 5$ μm with thin shell thickness ≈0.1 μm [11]. The experimental values of $a_{p,opt}/a$ in DSPs were rather close to those in ISPs for relatively large values of a. Fig. 4 verifies our results with marks corresponding to experimental data on observation of hollow Cu MTPs attributed to stress relaxation processes. In fact, the theoretical curves go very closely to the experimental points for all MTP types under consideration.

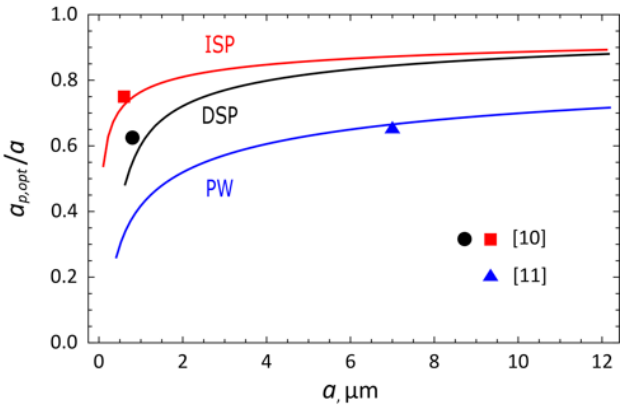

Fig. 4. (Color online) The dependence of the normalized optimal radius of the pore $a_{p,opt}/a$ on the final radius a of different MTPs in pure Cu: DSP (black curve), ISP (red curve) and PW (blue curve). The experimental points (≈0.8 μm, 0.63) and (≈0.6 μm, 0.75) correspond to hollow DSP and ISP, respectively, [10], while the experimental point (≈7 μm, 0.66) corresponds to hollow PW [11].

4. Summary and conclusions

In summary, a theoretical model has been suggested which describes the formation of central spherical pores in DSPs within a quasi-equilibrium energetic approach. The change in the total energy of a DSP in its initially solid and finally hollow states has been calculated under the assumption (proved in [9]) that the contributions of the twin boundary energy and the surface-tension strain energy are small as compared with those of the bulk-strain and free-surface energies, and can be neglected. The strain energy of a hollow DSP has been found as the work spent to create a positive partial WD of strength $\omega \approx 0.128$ rad (≈7°20′), piercing an elastic spherical shell, in its own stress field. We have also compared the normalized strain energies of different hollow MTPs (DSPs, ISPs and PWs) and demonstrated that hollow DSPs store higher strain energies with respect to solid DSPs, than hollow ISPs and PWs with respect to their solid counterparts, for the same inner to outer radii ratios. The surface energy change due to the pore formation has been calculated with taking into account the real polyhedral shape of hollow DSPs. Our analysis of the total energy change in a DSP due to a central pore formation showed that the latter becomes an effective channel of strain relaxation when the outer DSP radius exceeds a certain critical value $a_{0,cr}$. Our numerical estimates of $a_{0,cr}$ are in a good accordance with experimental observation of nanohole instability (collapse) in Ag and Au DSPs of 30 – 40 nm in diameter [21, 22] and pore presence in large Cu DSPs of 1 μm in diameter [10]. Besides, we have showed that, in large MTPs (with $a \gg 2$ μm), the normalized optimal radius $a_{p,opt}/a$ of a pore smoothly grows with the MTP size a. This means that large solid MTPs should tend to relieve their strain energy through their transformation in thin multiply twinned shells as was observed experimentally in Cu MTPs [10]. Moreover, our theoretical estimates of the optimal pore radius in DSPs and ISPs are in good agreement with experimental data on hollow Cu MTPs.

Acknowledgments. This work was supported by the grant of Russian Science Foundation No. 19-19-00617.

References

1. B. D. Anderson, J. B. Tracy. Nanoscale. 6, 12195 (2014). Crossref
2. X. Wang, J. I. Feng, Y. Bai, Q. Zhang, Y. Yin. Chem. Rev. 116, 10983 (2016). Crossref
3. L. Yu, X. Y. Yu, X. W. Lou. Adv. Mater. 30, 1800939 (2018). Crossref
4. M. Zhu, J. Tang, W. Wei, S. Li. Mater. Chem. Frontiers. 4, 1105 (2020).
5. I. V. Belova, A. V. Evteev, E. V. Levchenko, G. E. Murch. J. Nano Res. 7, 19 (2009). Crossref
6. A. P. Puente, D. Erdeniz, J. L. Fife, D. C. Dunand. Acta Mater. 103, 534 (2016). Crossref

7. K.N. Tu, U. Gösele. Appl. Phys. Lett. 86, 093111 (2005). Crossref
8. M. Vara, X. Wang, J. Howe, M. Chi, Y. Xia. ChemNanoMat. 4, 112 (2018). Crossref
9. A.E. Romanov, I.A. Polonsky, V.G. Gryaznov, S.A. Nepijko, T. Junghanns, N.J. Vitrykhovski. J. Crystal Growth. 129, 691 (1993). Crossref
10. I.S. Yasnikov, A.A. Vikarchuk. JETP Lett. 83, 42 (2006). Crossref
11. I.S. Yasnikov, A.A. Vikarchuk. Phys. Solid State. 48, 1433 (2006). Crossref
12. I.S. Yasnikov. Phys. Solid State. 49, 1224 (2007). Crossref
13. N.M. Vlasov, Y.G. Dragunov. Tech. Phys. 58, 218 (2013). Crossref
14. I. Tsagrakis, I.S. Yasnikov, E.C. Aifantis. Mech. Res. Comm. 93, 159 (2018). Crossref
15. V.G. Gryaznov, J. Heydenreich, A.M. Kaprelov, S.A. Nepijko, A.E. Romanov, J. Urban. Cryst. Res. Technol. 34, 1091 (1999). Crossref
16. L.D. Marks, L. Peng. J. Phys.: Condens. Matter. 28, 053001 (2016).
17. X. Wang, L. Figueroa-Cosme, X. Yang, M. Luo, J. Liu, Z. Xie, Y. Xia. Nano Lett. 16, 1467 (2016). Crossref
18. L. Han, P. Xiong, J. Bai, S. Che. J. Am. Chem. Soc. 133, 6106 (2011). Crossref
19. Z. Jiang, Q. Zhang, C. Zong, B.J. Liu, B. Ren, Z. Xie, L. Zheng. J. Mater. Chem. 22, 18192 (2012). Crossref
20. H. Huang, L. Zhang, T. Lv, A. Ruditskiy, J. Liu, Z. Ye, Y. Xia. ChemNanoMat. 1, 246 (2015). Crossref
21. S. Tehuacanero-Cuapa, R. Palomino-Merino, J. Reyes-Gasga. Rad. Phys. Chem. 87, 59 (2013). Crossref
22. S. Tehuacanero-Cuapa, J. Reyes-Gasga, E.F. Brès, R. Palomino-Merino, R. García-García. Rad. Eff. Def. Solids. 169, 838 (2014). Crossref
23. A.E. Romanov, V.I. Vladimirov. In: Dislocations in Solids. Vol. 9 (Ed. by F.R.N. Nabarro). Amsterdam, North-Holland Publ. Co (1992) pp. 191–402.
24. A.E. Romanov, A.L. Kolesnikova. Prog. Mater. Sci. 54, 740 (2009). Crossref
25. R. De Wit. J. Phys. C. Solid State Phys. 5, 529 (1972). Crossref
26. J.M. Galligan. Scr. Metall. 6, 161 (1972). Crossref
27. A.E.H. Love. A Treatise on the Mathematical Theory of Elasticity, 4th ed. New York, Dover (1944) 662 p.
28. A.I. Lurie. Theory of Elasticity. Berlin, Heidelberg, Springer-Verlag (2005) 1050 p.
29. I.A. Polonsky, A.E. Romanov, V.G. Gryaznov, A.M. Kaprelov. Philos. Mag. A. 64, 281 (1991). Crossref
30. A.L. Kolesnikova, M.Yu. Gutkin, A.V. Proskura, N.F. Morozov, A.E. Romanov. Int. J. Solids Structures. 99, 82 (2016). Crossref
31. A.I. Mikhailin, A.E. Romanov. Sov. Phys. Solid State. 28, 337 (1986).
32. Handbook of Physical Quantities (ed. by I.S. Grigoriev, E.Z. Meilikhov). Boca Raton, CRC Press (1996) 1568 p.
33. L. Vitos, A.V. Ruban, H.L. Skriver, J. Kollár. Surf. Sci. 411, 186 (1998). Crossref
34. M.Yu. Krauchanka, S.A. Krasnitckii, M.Yu. Gutkin, A.L. Kolesnikova, A.E. Romanov, E.C. Aifantis. Scr. Mater. 146, 77 (2018). Crossref